5-2023

# Exploring Surface-Induced Protein Folding of Amyloidogenic Proteins on Neuronal Membrane Surfaces using Molecular Dynamics Simulations

Amber Lewis
*Trinity University*, alewis2@trinity.edu

# EXPLORING SURFACE-INDUCED PROTEIN FOLDING OF AMYLOIDOGENIC PROTEINS ON NEURONAL MEMBRANES SURFACES USING MOLECULAR DYNAMICS SIMULATIONS

AMBER LEWIS

A DEPARTMENTAL SENIOR THESIS SUBMITTED TO THE
DEPARTMENT OF NEUROSCIENCE AT TRINITY UNIVERSITY
IN PARTIAL FULFILLMENT OF THE REQUIREMENTS FOR GRADUATION
WITH DEPARTMENTAL HONORS.

APRIL 14, 2023

THESIS ADVISOR

DEPARTMENT CHAIR

Jennifer Henderson, AVPAA

**Student Agreement**

I grant Trinity University (“Institution”), my academic department (“Department”), and the Texas Digital Library ("TDL") the non-exclusive rights to copy, display, perform, distribute and publish the content I submit to this repository (hereafter called "Work") and to make the Work available in any format in perpetuity as part of a TDL, digital preservation program, Institution or Department repository communication or distribution effort.

I understand that once the Work is submitted, a bibliographic citation to the Work can remain visible in perpetuity, even if the Work is updated or removed.

I understand that the Work's copyright owner(s) will continue to own copyright outside these non-exclusive granted rights.

I warrant that:

1) I am the copyright owner of the Work, or
2) I am one of the copyright owners and have permission from the other owners to submit the Work, or
3) My Institution or Department is the copyright owner and I have permission to submit the Work, or
4) Another party is the copyright owner and I have permission to submit the Work.

Based on this, I further warrant to my knowledge:

1) The Work does not infringe any copyright, patent, or trade secrets of any third party,
2) The Work does not contain any libelous matter, nor invade the privacy of any person or third party, and
3) That no right in the Work has been sold, mortgaged, or otherwise disposed of, and is free from all claims.

I agree to hold TDL, DPN, Institution, Department, and their agents harmless for any liability arising from any breach of the above warranties or any claim of intellectual property infringement arising from the exercise of these non-exclusive granted rights.”

**I choose the following option for sharing my thesis (required):**

[ ] Open Access (full-text discoverable via search engines)
[X] Restricted to campus viewing only (allow access only on the Trinity University campus via digitalcommons.trinity.edu)

**I choose to append the following Creative Commons license (optional):**

# Exploring Surface-Induced Protein Folding of Amyloidogenic Proteins on Neuronal Membrane Surfaces using Molecular Dynamics Simulations

Amber Lewis

Department of Neuroscience, Trinity University

## Author note

Email: alewis2@trinity.edu

Abstract

Self-aggregation and misfolding of two major amyloidogenic proteins, tau and human islet amyloid polypeptide (hIAPP), have been implemented in the pathogenesis of Alzheimer's disease, yet the exact mechanisms remain unknown. It has been suggested that the small oligomers are more toxic than mature fibrils, but the mechanisms of membrane disruption are unknown. Using molecular dynamics (MD) simulations, the membrane-binding and protein-folding behaviors of these amyloidogenic proteins were investigated. Using both coarse-grained (CG) and atomistic MD simulations, we successfully model protein oligomers binding to specific and non-specific lipid rafts and the subsequent surface-induced protein folding. The tau simulations revealed that the membrane binding deficient mutant k18 fragment experienced surface-induced helical conformations while the wild type k18 fragment did not, which may speak to the difference in toxicity. With hIAPP, we found that there was a significant difference in protein folding between the different model membranes, suggesting that nonspecific membranes are most likely to promote helical conformations. In addition, monomeric hIAPP is less likely to experience formation of ordered structures when bound to GM1. The hybrid system did not demonstrate any preferential folding based on model membrane or size of oligomer. In general, this study provides new mechanistic insights about the protein folding of membrane-bound amyloidogenic proteins.

*Keywords:* molecular dynamics, lipid rafts, tau, hIAPP, protein-folding

# Introduction

## Amyloidogenic Proteins: Tau

Human tau, a microtubule-associated protein, is widely known for its role in the development of several neurodegenerative diseases, including Alzheimer's Disease (AD) (Press-Sandler, 2018; Gerson, 2017). Hyperphosphorylated tau forms neurofibrillary tangles (NFTs), made of ordered beta-sheet rich tau fibrils, which are a major histopathological marker of AD (Fitzpatrick, 2017; Gerson, 2014). Hyperphosphorylated tau proteins are unable to maintain or assemble microtubules, and can even disrupt microtubules, thus causing neurodegeneration over time (Iqbal, 2010). Yet recent studies suggest that it is much smaller tau oligomers that pose the highest threat to neurons, specifically in the way they bind to neuronal membranes (Bok, 2021; Niewiadomska, 2021; Shafiei, 2017). Tau is a class of intrinsically disordered protein (IDP) which makes experimental studies of tau difficult (Nguyen, 2021). MD research thus far has focused on tau within solution, there has been little research on how tau folds when bound to a neuronal membrane. For our purposes, a 130-residue long fragment of tau, called k18, which represents the microtubule-binding domain of the protein was used. The wild type k18 fragment, or WT-k18, contains 4 repeated domains (R1, R2, R3, and R4) that are known to bind to membrane lipids (Sallaberry, 2021). We also created a mutated version of k18 with 3 amino acids changed to reduce the hydrophobicity of the protein and thus the binding affinity, hereby referred to as membrane binding deficit k18, or MBD-k18, based on the experimental discovery of Ait-Bouziad, 2017.

## Amyloidogenic Proteins: hIAPP

hIAPP is a hormone co-secreted with insulin from pancreatic beta-cells (Khemtemourian, 2022). Under normal circumstances, hIAPP has many functions including regulation of glucose

levels, vasodilation, bone resorption, renin activity, and slowing gastric emptying and glucagon release (Hassan, 2022). With hIAPP fibrillar aggregates found in 90% of patients with type 2 diabetes (T2D), these microscopic beta-sheet-rich fibrils have become a major histopathological marker of T2D (Milardi, 2021). It has been linked to the progression of T2D as well as neurodegenerative disorders such as Parkinson's disease and AD, and there is even a comorbidity, in which roughly 30% of individuals with AD also suffer from type II diabetes (Jackson, 2013; Ly, 2017; Khemtemourian, 2022). Similar to tau and amyloid beta, experimental studies have shown that oligomerized hIAPP is toxic to neurons via membrane damage (Jackson, 2013; Engel, 2008). In addition, it is thought that the small oligomers are more toxic than mature fibrils, but the detailed molecular mechanism of disordered hIAPP oligomers on neuronal membranes is still unknown (Mirzabekov, 1996; Willbold, 2021). We generated a full 37-residue long hIAPP monomer based on the published cryoEM fibrillar pentamer (Cao, 2020).

This project uses computational analysis of the MD simulations of these proteins within a system (complete with lipid membrane, solvent, and ions) to achieve a better understanding of how surface-induced folding contributes to the development of neurodegenerative diseases.

**Amyloidogenic Proteins: Interaction effects**

This project also investigates the interaction of tau and hIAPP, as it has not been well studied and there have been conflicting results of recent studies. A 2021 study found that hIAPP induces tau phosphorylation and aggregation in transgenic mice (Wijesekara, 2021) and a 2022 study showed similar results (Zhang, 2022), but a 2023 study found that hIAPP can reduce tauopathy (Yang, 2023).

### Lipid Rafts

Experimental studies have shown that the distribution of lipids in cell membranes are highly heterogeneous and contain phase-separated nanodomains, or lipid rafts, on both leaflets (Cebecauer, 2018; Sezgin, 2017). It has also been shown that both hIAPP and tau can attack either the inner or outer leaflet of the membrane, so it is necessary for us to study both (Westermark, 2011; Pooler, 2013). Thus, we used a control raft (CO-raft), a modified CO-raft containing ganglioside to mimic the outer leaflet of neurons (GM-raft), and a modified CO-raft containing phosphatidylserine-clusters to mimic the inner leaflet of any cell type (PS-raft) (Cheng, 2022). The CO-raft is a three-component lipid bilayer containing cholesterol, saturated phosphatidylcholine (PC), and unsaturated PC (Cheng, 2022). The model rafts also contain phase-separated liquid-ordered (Lo), liquid-disordered (Ld), and mixed Lo/Ld (Lod) domains on both outer and inner leaflet. The Lo domain mimics the ordered, cholesterol- and saturated PC enriched region, Ld mimics the disordered, saturated PC-enriched and cholesterol-depleted region, and Lod mimics the boundary region between the two, with characteristics of both (Cebecauer, 2018; Risselada, 2008; Cheng, 2022).

## Method

### MD Simulations

#### *Amyloidogenic Proteins*

All analyses were conducted with hIAPP (37 residues) and 2 tau variants, all of which were experimentally derived: tau-k18 wildtype (130 residues), and tau-k18 with three point mutations (V287E, I308E, and V318E) that make it less toxic, called MBD-k18, or membrane binding deficit (130 residues long) (Ait-Bouziad, 2017; Nguyen, 2021). The k18 segment was created by adding $Tau_{243\text{-}307}$ to the N-terminus of the fibril core, which was extracted by isolating

$Tau_{308-372}$ from chain A of the cryoEM pentamer (Fitzpatrick, 2017), in a random coil configuration, as demonstrated in Figure 1. The structure for hIAPP is extracted from a published cryoEM fibrillar pentamer structure as shown in Figure 2 (Cao, 2020). For both, the initial structure was in atomistic resolution but converted to CG resolution in order to reduce simulation time for aggregation and binding.

For the hybrid system consisting of both tau and hIAPP, hereby referred to as TAM (tau and amylin), a dimer was created with tau as chain A and hIAPP as chain B, as well as a tetramer with tau as chains B and C and hIAPP as chains A and D.

***Design of disordered tau and hIAPP oligomers in solution***

Disordered monomers were added to a simulation box and then solvated in 0.1 M NaCl and underwent energy minimization and position-restraints. For hIAPP, the initial extracted monomer was structured, so it was allowed to naturally collapse over 5 μs of CG MD simulation, as demonstrated in Figure 4A. Oligomers were created by adding multiple non-structured monomers (2 or 4) of the protein equally spaced out within the simulation box, then allowed to self-aggregate over 5 μs of CG MD simulation. This process is demonstrated in Figure 3 for a tau tetramer and in Figure 4B and 4C for hIAPP aggregates.

***Design of neuronal membrane mimics (lipid rafts)***

Three highly dynamic and heterogeneous lipid bilayers or lipid rafts, containing saturated and unsaturated phosphatidylcholine (PC), cholesterol, with or without anionic lipids, phosphatidylserine (PS) or ganglioside (GM1), were used to mimic the neuronal membranes (Ingolfsson, 2017). Specifically, the symmetric lipid raft (CO-raft) contains saturated DPPC, unsaturated DLPC, and cholesterol, and exhibits liquid-ordered (Lo), liquid-disordered (Ld), and mixed Lo/Ld domain boundaries. The other two lipid rafts, PS-raft and GM-raft, are asymmetric

lipid membranes in which PS- and GM-clusters are embedded on the Lod and Lo domain, respectively, on only one leaflet of the lipid membranes. Overall, the CO-raft represents the lipid membrane patch found on both leaflets of cell membranes. However, the PS-clusters represent biomarkers found on the intra-membrane leaflet facing the cytosol of any cell type (Kay, 2019), and the GM-clusters, specifically GM1, are biomarkers found on the extra-membrane leaflet on the surface of the neurons.

***Binding of oligomers on lipid rafts***

Binding of oligomers was initiated by placing the oligomer ~ 2 nm above the surface of each lipid raft. Three different initial positions of each oligomer, i.e., at the center and +/- 2 nm shifted along the x-direction, were created. For systems in which binding did not occur or was not stable within 15 microseconds, additional simulations with the protein starting +/- 2 nm in the y- or z-direction were created. Microsecond CG MD simulations were subsequently performed until the oligomer was bound to the membrane and stable.

***Atomistic simulations***

After the CG simulations, we have created atomistic structures of the membrane-bound oligomers on all three lipid rafts using a reverse-mapping procedure. We conducted 200 ns of atomistic simulation for both tau variants and 300 ns for hIAPP. We currently have 100 ns of data for the TAM hybrid system.

**Secondary Structure Analysis**

An analysis of the secondary structure/protein folding of every amino acid residue for every timestep was made using the gromacs function, *do_dssp*, which implements the original DSSP function (define secondary structure of proteins) (Anderson, 2022; Van Der Spoel, 2005). An analysis of the fraction of each type of secondary structure at each timestep was also

generated. The secondary structures were regrouped into four broader categories: 1) random, consisting of non-hydrogen bonded secondary structures such as coil and bend, 2) turn, 3) helix, which includes 3-helix, 5-helix, and alpha-helix, and 4) beta, which combines the planar conformations: beta-sheets and beta-bridges. The fraction of residues in each category was calculated to evaluate the net effect of the lipid domain on the folding behaviors or kinetics of hIAPP.

## Results

### Tau Protein Folding

The DSSP algorithm was used to identify the secondary structures of the WT-k18 and MBD-k18 tetramers on all three different raft surfaces. Transitions from disordered to ordered structures were seen within the 200 ns of simulation in various sections of the protein chains, with most of the ordered structures, specifically beta-sheets and beta-bridges, being transient. However, there was no noticeable change in the overall fraction of secondary structure overtime, as is evident in Figure 5B. Significant beta-sheet formation, shown as deep red lines in the DSSP plot in Figure 5A, was identified in one replicate of MBD-k18 and one replicate of WT-k18, both showing three out of the four chains participating in either inter-chain or intra-chain beta-sheet formation. The replicate-averaged secondary structure for each system is shown in Figure 6. A two-way ANOVA found that there was a strong significant effect of tau type, WT-k18 versus MBD-k18, on the amount of helical conformations ($F = 91.825$, $p < 0.001$), as well as a significant effect of tau type on the amount of random conformations ($F = 36.05$, $p < 0.001$). There was no statistically significant difference in the amount of planar structures (beta-sheets or beta-bridges) identified in WT-k18 compared to MBD-k18 ($F = 1.779$, $p = 0.207$), but they generally appeared more transient in MBD-k18 than in WT-k18 based on the DSSP colormap.

VMD was used to visualize the beta-sheets present at the end of the 200 ns simulation as well as the annular lipids in Figure 5C. (Cheng, 2022)

**hIAPP Protein Folding**

Same as with tau, the DSSP algorithm was used to calculate the time evolution and residue-resolved protein secondary structures of hIAPP oligomers on the raft membrane. During the 300 ns of simulation, some regions of the protein transitioned from non-hydrogen bonded, disordered structures to hydrogen-bonded, ordered structures, such as turn, helical, or planar beta, with this pattern being most prominent on CO-raft, shown in Figure 7A. The appearance of some ordered structures was transient, particularly helical structures in the dimer and tetramer. The fraction of residues in each of the four broader categories was calculated, shown in Figure 7B, to evaluate the net effect of the lipid domain on the folding behaviors or kinetics of hIAPP. The protein-folding kinetics showed a decrease in the disordered random structure and an increase in the ordered structures for all replicates on CO-raft. Beta structures were found for both the dimer and tetramer on CO-raft, but the monomer showed no beta structures at all, however a one-way ANOVA showed that the difference between the three oligomer sizes was not statistically significant ($F = 2.943$, $p = 0.129$). In addition, a decrease in the level of surface-induced helical structures was observed for the dimer and tetramer. The final 300 ns secondary structures of the representative replicate 1 for hIAPP oligomers on CO-raft are demonstrated in Figure 7. The average fraction of each secondary structure over three independent replicates for each oligomer is shown in Figure 8. (Lewis, 2023)

A one-way ANOVA of hIAPP on PS-raft revealed no significant differences between oligomer sizes for any of the secondary structures. However, there is a visible pattern that

suggests the amount of helical conformations increases as the oligomer size increases, although it is not statistically significant.

A one-way ANOVA of hIAPP on GM-raft revealed a significant difference in the helical conformations between the different oligomer sizes ($F = 7.186$, $p = 0.026$), specifically between the monomer and tetramer. It also showed the same pattern of helical conformations increasing as the oligomer size increases as the PS-raft did.

Next, a two-way ANOVA was used to determine the effects of raft-type as well as oligomer size on the amount of specific secondary structures, as well as any interaction effect of raft-type and oligomer size. It revealed that there was a small significant effect of raft type on the amount of helices ($F = 4.74$, $p = 0.022$), with CO-raft having significantly more helical conformations. There was also a significant interaction effect of raft and oligomer on the amount of helices ($F = 4.553$, $p = 0.010$), as the CO-raft monomer had a larger amount than the dimer or tetramer, but there was a non-significant effect of oligomer size alone on helices ($F = 3.478$, $p = 0.053$).

**TAM**

The same DSSP algorithm was used for the 100 ns of simulation for the TAM system. DSSP plots for representative dimer and tetramer replicates on CO-raft are demonstrated in Figure 9, as well as the fraction of broader secondary structure groups over time. The data is still preliminary, as we hope to reach at least 200 ns of simulation for analysis. A two-way ANOVA found that there was a significant difference in the amount of random conformations between raft type ($F = 6.16$, $p = 0.014$), with GM-raft having the highest amount and PS-raft having the lowest, but there was not a significant difference in helical or beta conformations. Within the 100 ns, we do not see the same transition from disordered to ordered structures that was evident with

hIAPP, and there is very little change in overall fraction of secondary structure over time. Figure 10 shows the replicate- and time-averaged fraction of each secondary structure.

## Discussion

### Tau

For the tau tetramer system, both inter- and intra-chain beta-sheets were found, with MBD-k18 showing more transient beta-sheets than WT-k18. These results suggest membrane-assisted beta-sheet formation can be detected for large amyloid protein aggregates, as the tau k18 tetramer has 520 residues. However, longer simulation time would be required to further explore the role of membrane domains on beta-sheet formation. Our results corroborate recent experimental data that shows k18 can form beta-sheets on an anionic membrane surface, and our simulation provides evidence that not only can beta-sheets form on anionic membrane surfaces such as GM1, but they are likely to form (Majewski, 2020; Cheng, 2022).

The formation of beta-sheets on membrane-bound tau represents the early events of membrane damage, through mechanisms such as the pore, carpeting, or detergent-like models (Pooler, 2013). The greater amount of non-transient beta-sheet formation for WT-k18 compared to MBD-k18 implies that electrostatic interactions have an important role in membrane-induced protein folding. Due to their hydrophobicity, these beta-sheets may also facilitate further aggregation and attract other amyloidogenic proteins to create larger oligomers and more membrane damage (Richardson, 2002). Thus, the small beta-sheets observed in this study can act as a base for future work, both experimental and computational, to understand the nucleation process of tau on lipid membranes. (Cheng, 2022) There were no significant differences between the different raft systems, but there was a difference in the amount of helices and random coil between WT-k18 and MBD-k18. Specifically, almost no helical conformations were seen in

WT-k18. Interpreting this result proves to be a challenge. For tau, beta-sheets are the primary toxic-motif, known to facilitate protein aggregation, but one study found abnormal tau aggregates with a high proportion of helical conformations (Avila, 2006). Thus, the secondary structure analysis alone is not enough to suggest the increased toxicity of WT-k18 compared to MBD-k18, but in combination with binding affinity data we can draw that conclusion (Cheng, 2022).

**hIAPP**

A more prominent pattern of surface-induced protein folding was found in hIAPP than what was found in tau k18, with a transition from disordered to ordered hydrogen-bonded structures being evident in the time-dependent graphs, as shown in Figure 7B. For the CO-raft, we found a decrease in alpha-helix and increase in beta-sheets as the oligomers increased in size from monomer to dimer to tetramer, although not statistically significant. Figure 7C shows that one of the tetramers bound to CO-raft demonstrated a triple beta-sheet structure embedded into the lipid raft involving chain C and chain D. I hypothesize that this stable triple beta-sheet is the precursor to a beta-barrel, a recently modeled mechanism of pore formation and subsequent cell death, made of parallel and antiparallel beta-sheets (Sepehri, 2021; Sulatskaya, 2021). This ion channel pore formation has been confirmed experimentally with hIAPP and planar lipid membranes (Mirzabekov, 1996), and beta-barrel formation has been observed experimentally and computationally (Sun, 2019).

This study provides insights into the mechanisms of hIAPP aggregate binding behavior on various dynamic neuronal membrane mimics: a control, a general inner-leaflet mimic, and a neuronal outer-leaflet mimic. The surface-induced protein folding from disordered-to-ordered structures was seen in most replicates on all three surface types. In hIAPP, both helical and

planar conformations have been associated with membrane damage, specifically beta-barrels as well as alpha-helix barrels. For both GM-raft and CO-raft there was an increase in beta formation as the oligomer size increased, although not statistically significant, and for GM-raft and PS-raft there was an increase in helical conformations as oligomer size increased, which was statistically significant for GM-raft. This suggests that hIAPP monomers experience little-to-no protein folding on GM1, and larger oligomers are necessary to see surface-induced protein folding. In comparison, monomers on CO-raft showed no beta formation, but large amounts of helical conformation. Thus a monomer on CO-raft is unlikely to see beta-sheet formation and is more likely to see helical conformation.

**TAM**

For the TAM system, we observed no significant changes in protein folding by oligomer size or raft type. This could suggest either that the system did not experience significant surface-induced folding, or it could suggest that the folding became highly stabilized after binding. There were also no significant differences between the amounts of secondary structure by raft type or oligomer size, but all systems did experience some beta and helical conformations, which implies that for the TAM there is no preferential protein-folding, and any raft type or oligomer size is equally likely to result in surface induced protein folding. Although we cannot draw a definitive conclusion from these preliminary results, we hope that in combination with other simulation analysis conducted in our lab these findings will contribute to this new area of investigation.

It is important to note that there is likely a lower binding affinity for the TAM system than either individual system because far more initial CG simulations had to be done in order to find stabilized binding.

**Limitations and Future Directions**

When doing any MD studies there are several limitations. Firstly, it takes a large amount of computational power and time to run simulations, especially in atomistic resolution. Running coarse-grained simulations, we were able to get ~2-3 microseconds of simulation per day, but with atomistic it is only ~2 nanoseconds per day. However, with the Leviosa cluster at Trinity, it is not possible to improve the speed of our simulations. Thus, our atomistic simulation can only look at initial binding. In addition, all MD studies rely on the use of force fields, and the force field chosen can impact the results. For CG simulation, we use the MARTINI-2 force-field, and for atomistic simulation the AMBER99SB and Slipids, neither of which may be appropriate for investigating protein-protein and protein-lipid interactions of IDPs, but there is not currently any better available force field.

Our lab has recently implemented machine learning algorithms to quantify the amount of membrane damage caused by the amyloidogenic proteins, and we hope to integrate these findings with the protein folding data to better understand the effects of specific secondary structure on the membrane. As of now, we currently only have atomistic simulation for the WT-k18 tetramers therefore the next step in order to fully understand the hybrid system will be to create a simulation for the WT-k18 dimer and monomer. Finally, the end goal for much of MD amyloidogenic protein research is to develop drug therapies to prevent the aggregation of the proteins or the membrane damaging mechanisms in order to treat AD or T2D.

## References

Ait-Bouziad, N., Lv, G., Mahul-Mellier, A. L., Xiao, S., Zorludemir, G., Eliezer, D., . . . Lashuel, H. A. (2017). Discovery and characterization of stable and toxic Tau/phospholipid oligomeric complexes. *Nat Commun, 8*(1), 1678. doi:10.1038/s41467-017-01575-4

Andersen, C. A., Palmer, A. G., Brunak, S., & Rost, B. (2002). Continuum secondary structure captures protein flexibility. *Structure, 10*(2), 175-184. doi:10.1016/s0969-2126(02)00700-1

Avila, J., Santa-Maria, I., Perez, M., Hernandez, F., & Moreno, F. (2006). Tau phosphorylation, aggregation, and cell toxicity. *J Biomed Biotechnol, 2006*(3), 74539. doi:10.1155/JBB/2006/74539

Bok, E., Leem, E., Lee, B. R., Lee, J. M., Yoo, C. J., Lee, E. M., & Kim, J. (2021). Role of the Lipid Membrane and Membrane Proteins in Tau Pathology. *Front Cell Dev Biol, 9*, 653815. doi:10.3389/fcell.2021.653815

Cao, Q., Boyer, D. R., Sawaya, M. R., Ge, P., & Eisenberg, D. S. (2020). Cryo-EM structure and inhibitor design of human IAPP (amylin) fibrils. *Nat Struct Mol Biol, 27*(7), 653-659. doi:10.1038/s41594-020-0435-3

Cebecauer, M., Amaro, M., Jurkiewicz, P., Sarmento, M. J., Sachl, R., Cwiklik, L., & Hof, M. (2018). Membrane Lipid Nanodomains. *Chem Rev, 118*(23), 11259-11297. doi:10.1021/acs.chemrev.8b00322

Cheng, K. H., Graf, A., Lewis, A., Pham, T., & Acharya, A. (2022). Exploring Membrane Binding Targets of Disordered Human Tau Aggregates on Lipid Rafts Using Multiscale Molecular Dynamics Simulations. *Membranes (Basel), 12*(11). doi:10.3390/membranes12111098

Engel, M. F., Khemtemourian, L., Kleijer, C. C., Meeldijk, H. J., Jacobs, J., Verkleij, A. J., . . . Hoppener, J. W. (2008). Membrane damage by human islet amyloid polypeptide through fibril growth at the membrane. *Proc Natl Acad Sci U S A, 105*(16), 6033-6038. doi:10.1073/pnas.0708354105

Fitzpatrick, A. W. P., Falcon, B., He, S., Murzin, A. G., Murshudov, G., Garringer, H. J., . . . Scheres, S. H. W. (2017). Cryo-EM structures of tau filaments from Alzheimer's disease. *Nature, 547*(7662), 185-190. doi:10.1038/nature23002

Gerson, J. E., Castillo-Carranza, D. L., & Kayed, R. (2014). Advances in therapeutics for neurodegenerative tauopathies: moving toward the specific targeting of the most toxic tau species. *ACS Chem Neurosci, 5*(9), 752-769. doi:10.1021/cn500143n

Gerson, J. E., Sengupta, U., & Kayed, R. (2017). Tau Oligomers as Pathogenic Seeds: Preparation and Propagation In Vitro and In Vivo. *Methods Mol Biol, 1523*, 141-157. doi:10.1007/978-1-4939-6598-4_9

Hassan, S., White, K., & Terry, C. (2022). Linking hIAPP misfolding and aggregation with type 2 diabetes mellitus: a structural perspective. *Biosci Rep, 42*(5). doi:10.1042/BSR20211297

Ingolfsson, H. I., Carpenter, T. S., Bhatia, H., Bremer, P. T., Marrink, S. J., & Lightstone, F. C. (2017). Computational Lipidomics of the Neuronal Plasma Membrane. *Biophys J, 113*(10), 2271-2280. doi:10.1016/j.bpj.2017.10.017

Iqbal, K., Liu, F., Gong, C. X., & Grundke-Iqbal, I. (2010). Tau in Alzheimer disease and related tauopathies. *Curr Alzheimer Res, 7*(8), 656-664. doi:10.2174/156720510793611592

Jackson, K., Barisone, G. A., Diaz, E., Jin, L. W., DeCarli, C., & Despa, F. (2013). Amylin deposition in the brain: A second amyloid in Alzheimer disease? *Ann Neurol, 74*(4), 517-526. doi:10.1002/ana.23956

Kay, J. G., & Fairn, G. D. (2019). Distribution, dynamics and functional roles of phosphatidylserine within the cell. *Cell Commun Signal, 17*(1), 126. doi:10.1186/s12964-019-0438-z

Khemtemourian, L., Fatafta, H., Davion, B., Lecomte, S., Castano, S., & Strodel, B. (2022). Structural Dissection of the First Events Following Membrane Binding of the Islet Amyloid Polypeptide. *Front Mol Biosci, 9*, 849979. doi:10.3389/fmolb.2022.849979

Lewis, A., Pham, T., Nguyen, N., Graf, A., & Cheng, K. H. (2023). Lipid domain boundary triggers membrane damage and protein folding of human islet amyloid polypeptide in the early pathogenesis of amyloid diseases. *Biophys Chem, 296*, 106993. doi:10.1016/j.bpc.2023.106993

Ly, H., Verma, N., Sharma, S., Kotiya, D., Despa, S., Abner, E. L., . . . Despa, F. (2021). The association of circulating amylin with beta-amyloid in familial Alzheimer's disease. *Alzheimers Dement (N Y), 7*(1), e12130. doi:10.1002/trc2.12130

Majewski, J., Jones, E. M., Vander Zanden, C. M., Biernat, J., Mandelkow, E., & Chi, E. Y. (2020). Lipid membrane templated misfolding and self-assembly of intrinsically disordered tau protein. *Sci Rep, 10*(1), 13324. doi:10.1038/s41598-020-70208-6

Milardi, D., Gazit, E., Radford, S. E., Xu, Y., Gallardo, R. U., Caflisch, A., . . . Ramamoorthy, A. (2021). Proteostasis of Islet Amyloid Polypeptide: A Molecular Perspective of Risk Factors and Protective Strategies for Type II Diabetes. *Chem Rev, 121*(3), 1845-1893. doi:10.1021/acs.chemrev.0c00981

Mirzabekov, T. A., Lin, M. C., & Kagan, B. L. (1996). Pore formation by the cytotoxic islet amyloid peptide amylin. *J Biol Chem, 271*(4), 1988-1992. doi:10.1074/jbc.271.4.1988

Nguyen, P. H., Ramamoorthy, A., Sahoo, B. R., Zheng, J., Faller, P., Straub, J. E., . . . Derreumaux, P. (2021). Amyloid Oligomers: A Joint Experimental/Computational Perspective on Alzheimer's Disease, Parkinson's Disease, Type II Diabetes, and Amyotrophic Lateral Sclerosis. *Chem Rev, 121*(4), 2545-2647. doi:10.1021/acs.chemrev.0c01122

Niewiadomska, G., Niewiadomski, W., Steczkowska, M., & Gasiorowska, A. (2021). Tau Oligomers Neurotoxicity. *Life (Basel), 11*(1). doi:10.3390/life11010028

Pooler, A. M., Polydoro, M., Wegmann, S., Nicholls, S. B., Spires-Jones, T. L., & Hyman, B. T. (2013). Propagation of tau pathology in Alzheimer's disease: identification of novel therapeutic targets. *Alzheimers Res Ther, 5*(5), 49. doi:10.1186/alzrt214

Press-Sandler, O., & Miller, Y. (2018). Molecular mechanisms of membrane-associated amyloid aggregation: Computational perspective and challenges. *Biochim Biophys Acta Biomembr, 1860*(9), 1889-1905. doi:10.1016/j.bbamem.2018.03.014

Richardson, J. S., & Richardson, D. C. (2002). Natural beta-sheet proteins use negative design to avoid edge-to-edge aggregation. *Proc Natl Acad Sci U S A, 99*(5), 2754-2759. doi:10.1073/pnas.052706099

Risselada, H. J., & Marrink, S. J. (2008). The molecular face of lipid rafts in model membranes. *Proc Natl Acad Sci U S A, 105*(45), 17367-17372. doi:10.1073/pnas.0807527105

Sallaberry, C. A., Voss, B. J., Majewski, J., Biernat, J., Mandelkow, E., Chi, E. Y., & Vander Zanden, C. M. (2021). Tau and Membranes: Interactions That Promote Folding and Condensation. *Front Cell Dev Biol, 9*, 725241. doi:10.3389/fcell.2021.725241

Sepehri, A., Nepal, B., & Lazaridis, T. (2021). Distinct Modes of Action of IAPP Oligomers on Membranes. *J Chem Inf Model, 61*(9), 4645-4655. doi:10.1021/acs.jcim.1c00767

Sezgin, E., Levental, I., Mayor, S., & Eggeling, C. (2017). The mystery of membrane organization: composition, regulation and roles of lipid rafts. *Nat Rev Mol Cell Biol, 18*(6), 361-374. doi:10.1038/nrm.2017.16

Shafiei, S. S., Guerrero-Munoz, M. J., & Castillo-Carranza, D. L. (2017). Tau Oligomers: Cytotoxicity, Propagation, and Mitochondrial Damage. *Front Aging Neurosci, 9*, 83. doi:10.3389/fnagi.2017.00083

Sulatskaya, A. I., Kosolapova, A. O., Bobylev, A. G., Belousov, M. V., Antonets, K. S., Sulatsky, M. I., . . . Nizhnikov, A. A. (2021). beta-Barrels and Amyloids: Structural Transitions, Biological Functions, and Pathogenesis. *Int J Mol Sci, 22*(21). doi:10.3390/ijms222111316

Sun, Y., Kakinen, A., Xing, Y., Faridi, P., Nandakumar, A., Purcell, A. W., . . . Ding, F. (2019). Amyloid Self-Assembly of hIAPP8-20 via the Accumulation of Helical Oligomers, alpha-Helix to beta-Sheet Transition, and Formation of beta-Barrel Intermediates. *Small, 15*(18), e1805166. doi:10.1002/smll.201805166

Van Der Spoel, D., Lindahl, E., Hess, B., Groenhof, G., Mark, A. E., & Berendsen, H. J. (2005). GROMACS: fast, flexible, and free. *J Comput Chem, 26*(16), 1701-1718. doi:10.1002/jcc.20291

Westermark, G. T., & Westermark, P. (2011). Localized amyloids important in diseases outside the brain--lessons from the islets of Langerhans and the thoracic aorta. *FEBS J, 278*(20), 3918-3929. doi:10.1111/j.1742-4658.2011.08298.x

Wijesekara, N., Goncalves, R. A., Ahrens, R., Ha, K., De Felice, F. G., & Fraser, P. E. (2021). Combination of human tau and islet amyloid polypeptide exacerbates metabolic dysfunction in transgenic mice. *J Pathol, 254*(3), 244-253. doi:10.1002/path.5674

Willbold, D., Strodel, B., Schroder, G. F., Hoyer, W., & Heise, H. (2021). Amyloid-type Protein Aggregation and Prion-like Properties of Amyloids. *Chem Rev, 121*(13), 8285-8307. doi:10.1021/acs.chemrev.1c00196

Yang, Y. Y., Ren, Y. T., Jia, M. Y., Bai, C. Y., Liang, X. T., Gao, H. L., Zhong, M. L., Wang, T., Guo, C. (2023). The human islet amyloid polypeptide reduces hippocampal tauopathy and behavioral impairments in P301S mice without inducing neurotoxicity or seeding amyloid aggregation. *Exp Neurol, 362*, 114346. doi:10.1016/j.expneurol.2023.114346

Zhang, G., Meng, L., Wang, Z., Peng, Q., Chen, G., Xiong, J., & Zhang, Z. (2022). Islet amyloid polypeptide cross-seeds tau and drives the neurofibrillary pathology in Alzheimer's disease. *Mol Neurodegener, 17*(1), 12. doi:10.1186/s13024-022-00518-y

# Figures

## Figure 1

*Tau WT-k18 and MBD-k18 Structure Extraction*

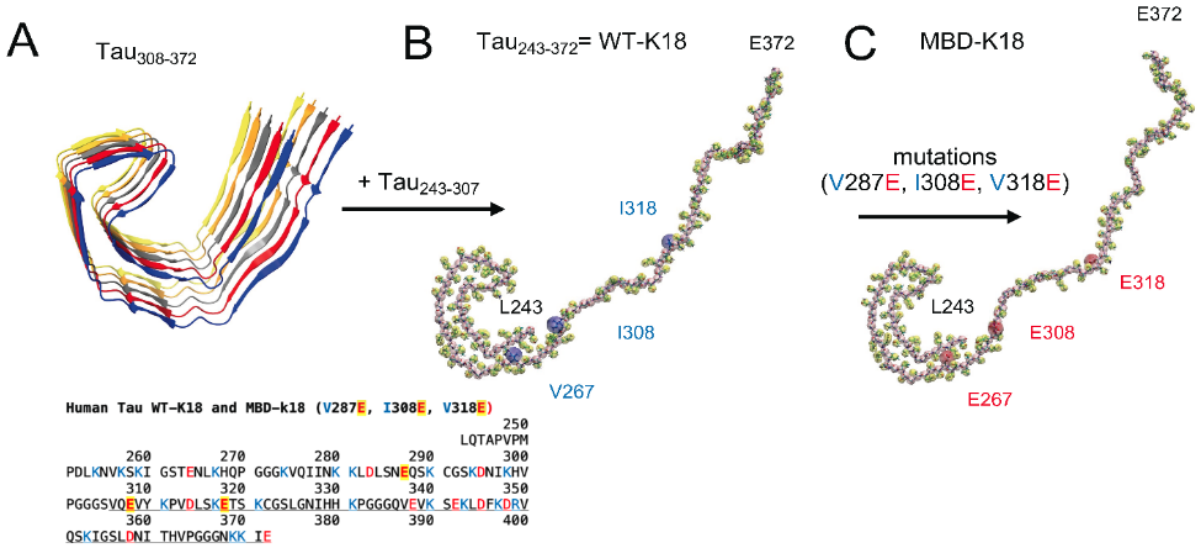


*Note*. A single chain from the (A) cryoEM tau pentamer structure was extracted and used to build the (B) atomistic wild type k18 (WT-k18) and (C) mutated k18 (MBD-k18) with the three point mutations identified. This figure is adopted from previous works (Cheng, 2022).

**Figure 2**

*hIAPP Structure Extraction*

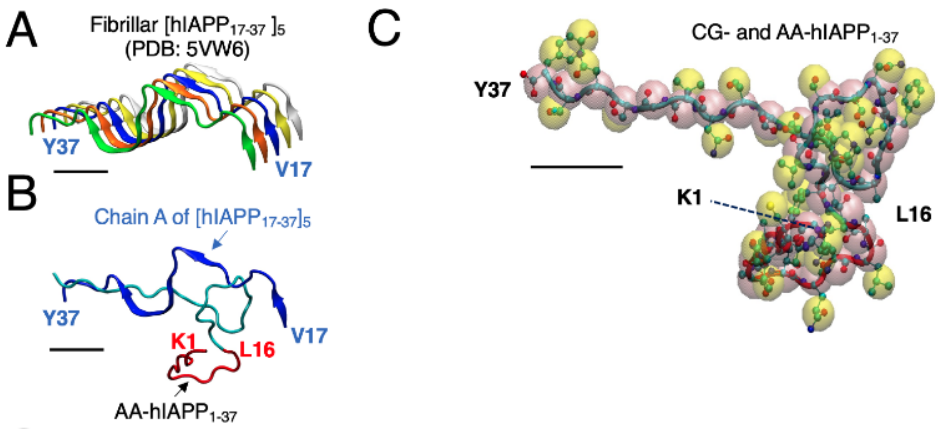


*Note*. A single chain from the (A) cryoEM tau pentamer structure was extracted and used to build the full-length atomistic hIAPP$_{1–37}$ (B) upon attaching a random AA-hIAPP$_{1–16}$ coil (red coil) to its N-terminus. Using an atomistic to coarse-grained spatial transformation procedure, the CG hIAPP1–37 structure shown with yellow beads for side chains and pink beads for backbones, is overlaid onto the AA-hIAPP1–37 shown with side chains in licorice and backbone in ribbon (C). A scale bar of 1 nm is given for each CG or AA structure. This figure is adopted from previous work (Lewis, 2023).

**Figure 3**

*Tau Tetramer Formation*

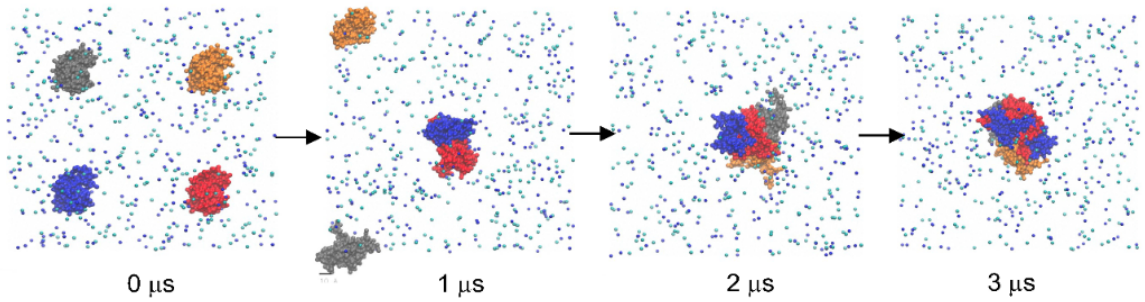


*Note*. The unbiased self-aggregation process of four WT-k18 monomers within 3 μs of CG simulation in 0.1 M NaCl. Water is represented as blue dots, Na + ions as dark blue spheres, and Cl- ions as light blue spheres. This figure is adopted from previous works (Cheng, 2022).

**Figure 4**

*hIAPP Collapse and Oligomer Formation*

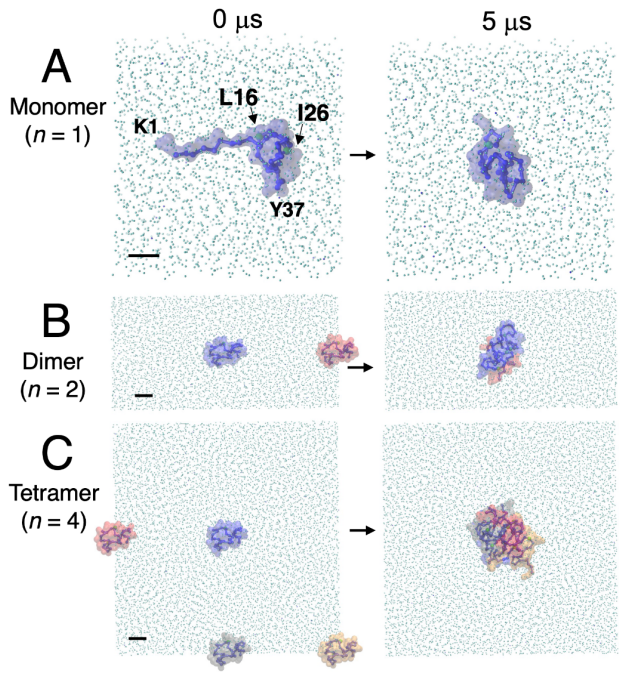


Note. (A) The CG hIAPP monomer before and after a 5-μs-long CG simulation are shown. The unbiased self-aggregation process of (B) two or (C) four identical equilibrated monomers from before and after a 5-μs-long CG simulation resulted in the formation of a dimer and tetramer. Water is represented as blue dots, Na + ions as dark blue spheres, and Cl- ions as light blue spheres. A scale bar of 1 nm is shown in each structure. This figure is adopted from previous work (Lewis, 2023).

**Figure 5**

*DSSP Plot, VMD Rendering, and Time-Averaged Secondary Structure for Tau*

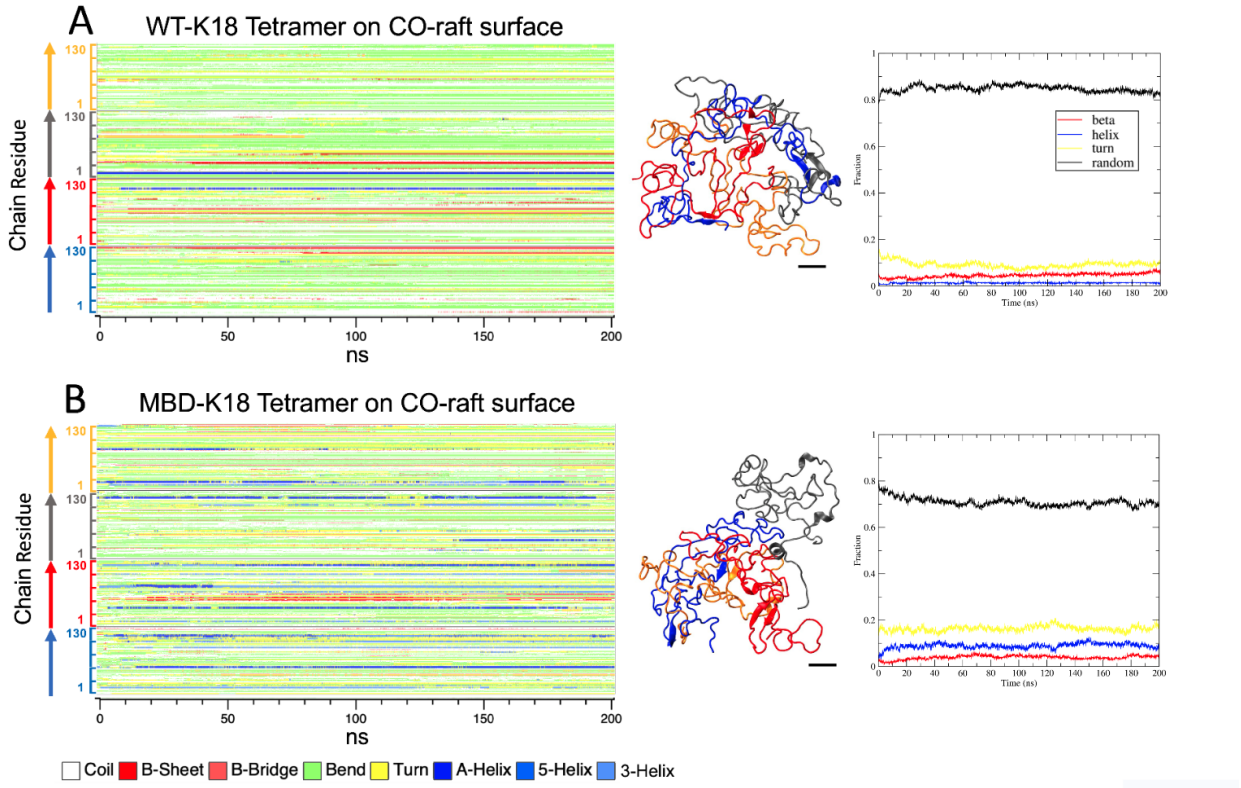


*Note*. Membrane-induced protein folding of tau k18 tetramers on CO-raft surfaces. The secondary structures of each residue within all 200 ns of simulation are shown for one replicate of (A) WT-k18 and (B) MBD-k18 on CO-raft. The fraction of residues that participated in each of the combined secondary structure groups over time are shown to the right. Within the middle of each panel the VMD visualization of the oligomers at the end of the simulation is shown. Each chain is color coded, chain A in blue, chain B in red, chain C in gray, and chain D in orange. The scale bar indicates 10 angstroms. This figure is adopted from previous works (Cheng, 2022).

**Figure 6**

*Time- and Replicate-Averaged Secondary Structure by Tau Type and Raft Type*

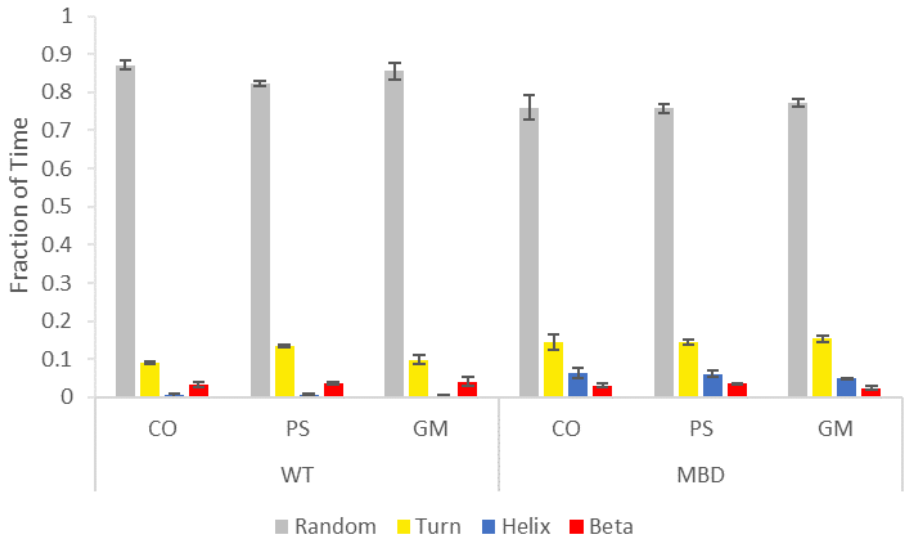


*Note*. Total protein secondary structures of membrane-bound WT-k18 and MBD-k18. The data represents the replicate-averaged fraction of time over the 200 ns that each secondary structure was present over three independent replicates for each raft-type and tau variant. The error bar represents the standard error of the mean.

**Figure 7**

*DSSP Plot, Time-Averaged Secondary Structure, and VMD Rendering for hIAPP*

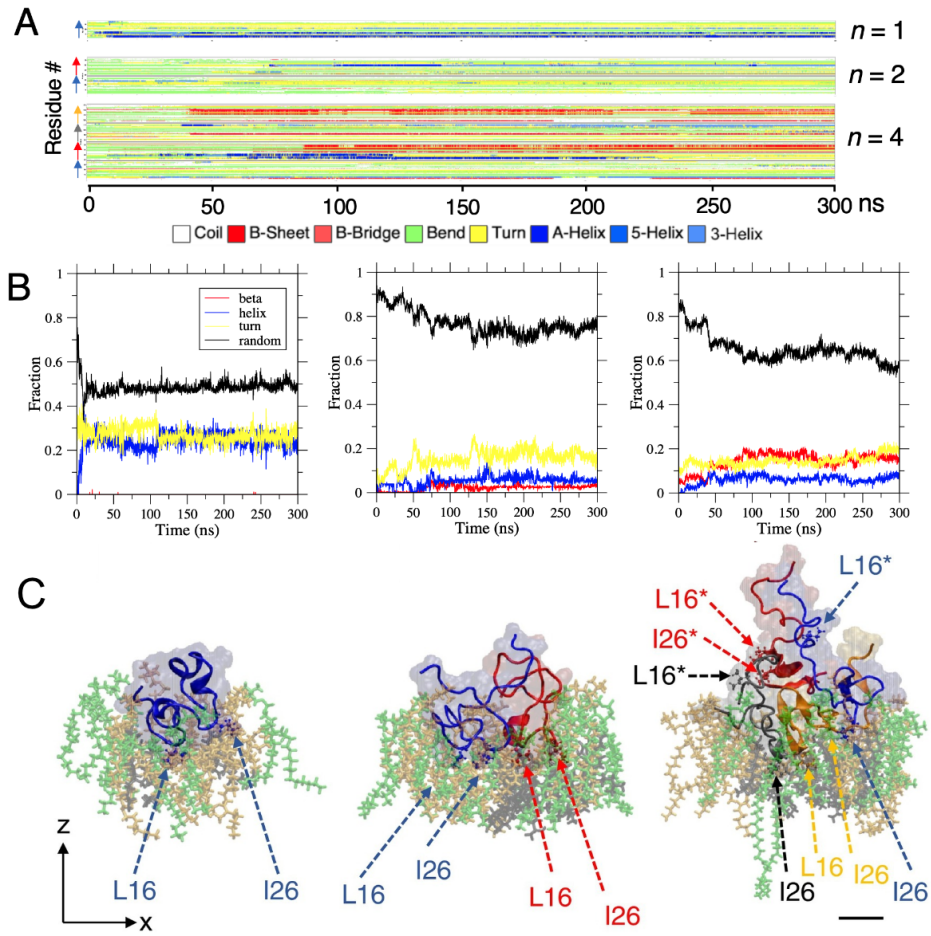


*Note*. (A) The secondary structures of each residue within all 300 ns of simulation are shown for representative replicates of the monomer, dimer, and tetramer on CO-raft. (B) The fractions of residues involved in beta, helix, turn, and random structures are also shown over time for each oligomer, left to right: monomer, dimer, tetramer. (C) VMD rendering of the protein and surrounding annular lipid, with the two primary hydrophobic residues, L16 and I26, labeled. Protein structures are shown in ribbons, highlighting the different secondary structures (random, helical, and beta-sheet) of each oligomer. This figure is adopted from previous work (Lewis, 2023).

**Figure 8**

*Time- and Replicate-Averaged Secondary Structure by Raft Type and Oligomer Size for hIAPP*

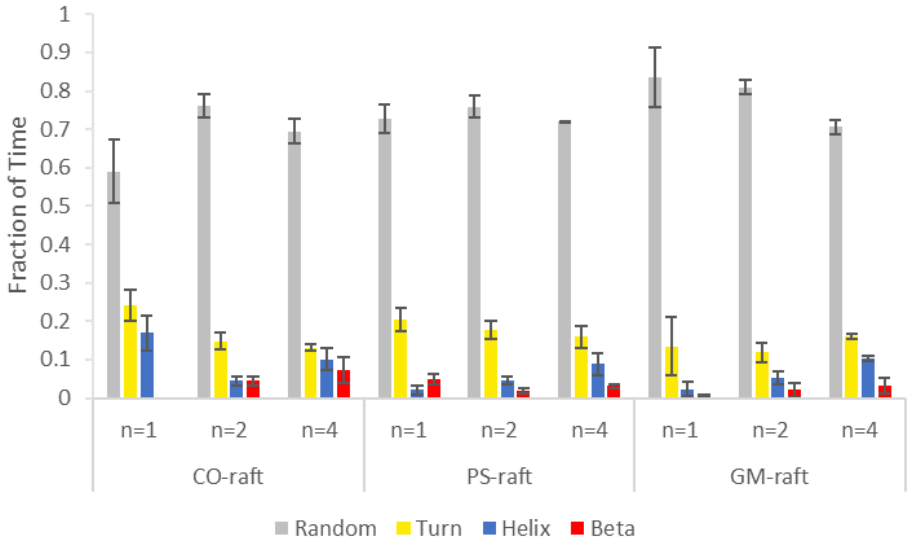


*Note*. Total protein secondary structures of membrane-bound hIAPP. The data represents the replicate-averaged fraction of time over the 300 ns that each secondary structure was present over three independent replicates for each oligomer size and raft-type. The error bars represent the standard error of the mean.

**Figure 9**

*DSSP Plot and Time-Averaged Secondary Structure for TAM*

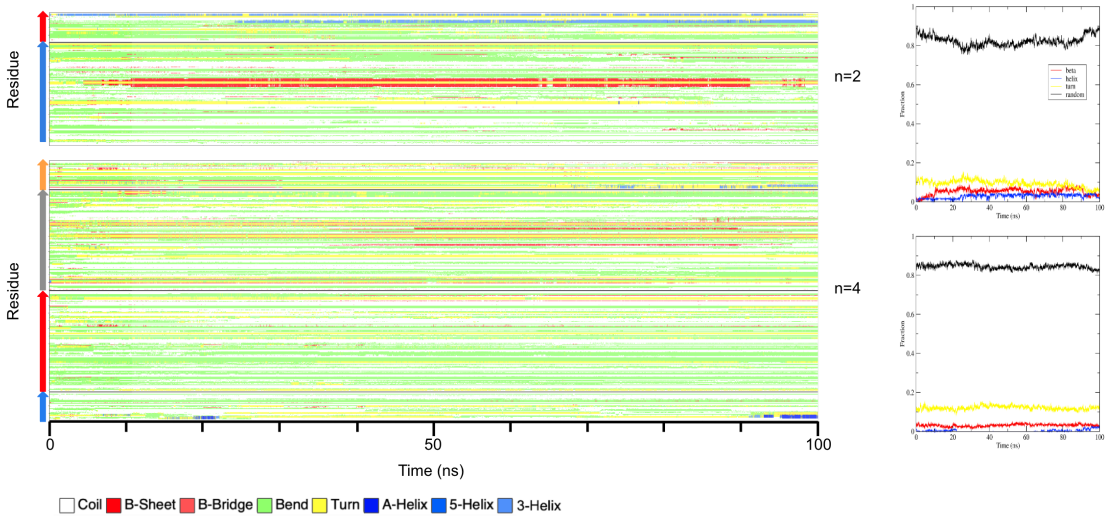


*Note*. The secondary structures of each residue within all 100 ns of simulation are shown for one replicate of a dimer and a tetramer on CO-raft. The fraction of residues that participated in each of the combined secondary structure groups over time for the specific replicates on CO-raft are shown to the right.

**Figure 10**

*Time- and Replicate-Averaged Secondary Structure by Raft Type and Oligomer Size for TAM*

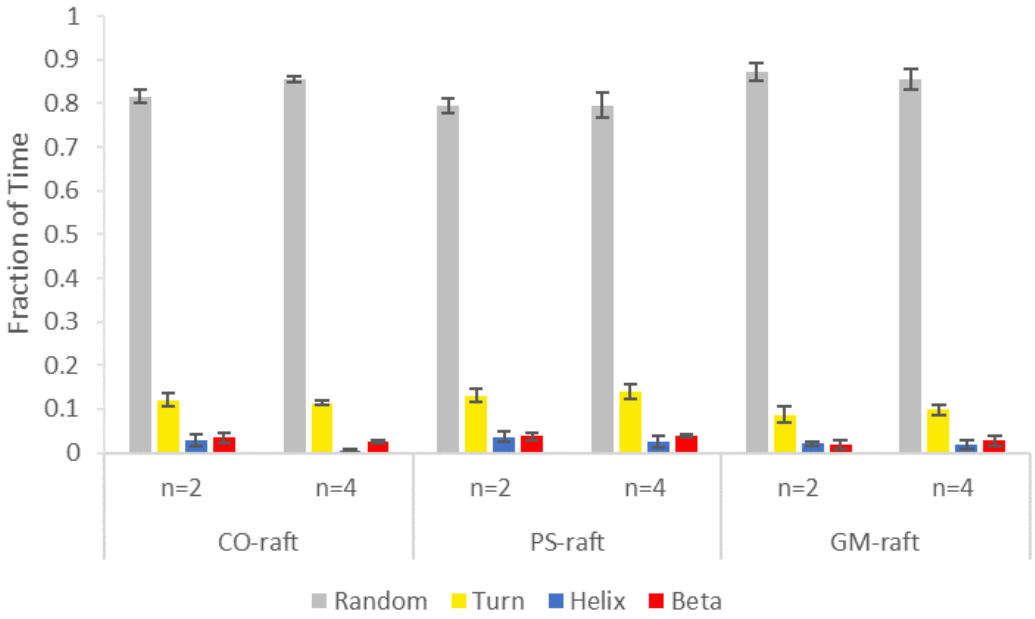


*Note.* Total protein secondary structures of membrane-bound TAM dimers and tetramers. The data represents the replicate-averaged fraction of time over the 100 ns that each secondary structure was present over three independent replicates for each oligomer size and raft-type. The error bars represent the standard error of the mean.